J. Fluid Mech. (1971), *vol.* 50, *part* 4, *pp.* 675–687
Printed in Great Britain

Rotating flow over a step

By DON L. BOYER
University of Delaware, Newark

(Received 21 December 1970 and in revised form 2 June 1971)

The flow of a rotating homogeneous incompressible fluid over a step is investigated. In the physical system considered the rotation axis is vertical and the step, which is assumed to be infinitely long, is located on a horizontal plane surface. Upstream of the step the fluid is in a uniform free stream motion at an angle α to a line perpendicular to the step axis. The analysis is restricted by the following: $E \ll 1$, $Ro \sim E^{\frac{1}{2}}$, $h/D \sim E^{\frac{1}{2}}$, $H/D \sim E^0$, and $\cos\alpha \sim E^0$ where Ro and E are the Rossby and Ekman numbers and h/D and H/D are the step height to step width and water depth to step width ratios respectively. The flow field is shown to consist of interior geostrophic regions, Ekman layers on the horizontal surfaces and vertical shear layers located in the vicinity of vertical planes defined by the edges of the step. In the vertical layers there is a balance between the inertial, Coriolis, and pressure terms in the momentum equations while the effects of viscosity are found to be negligible. Downstream of the step the streamlines are shifted to the right (positive or Northern Hemisphere rotation) of their upstream locations by a distance of $S = 2^{\frac{1}{2}}(h/D)E^{-\frac{1}{4}}\cos\alpha$. Experiments are presented which are in good agreement with the theory advanced.

1. Introduction

In a recent paper Boyer (1971) considered the flow of a homogeneous incompressible rotating fluid over a long ridge of constant cross-section (figure 1). The analysis and accompanying experiments in this study were restricted by the following:

$$\left.\begin{aligned} E = \nu/2\omega D^2 \ll 1, \quad Ro = U/2\omega D = kE^{\frac{1}{2}}, \\ h/D = h_0 E^{\frac{1}{2}}, \quad H/D \sim E^0, \quad \cos\alpha \sim E^0, \end{aligned}\right\} \tag{1.1}$$

where E is the Ekman number, ν the kinematic viscosity, ω the rotation rate, Ro the Rossby number, U the free stream speed, k and h_0 constants of order unity, α the angle between the free stream and the ridge axis, and where the remaining terms are defined in figure 1. In addition to (1.1), it was also assumed that the ridge slope is of infinitesimal order (i.e. $O(E^{\frac{1}{2}})$) everywhere.

The purpose of the present paper is to show how this latter requirement can be relaxed; i.e. while retaining (1.1), how does one analyze flows for which certain portions of the topography slope are large? In order to simplify the discussion while still including the pertinent physics for this class of problems, the flow over a step will be considered (figure 2).

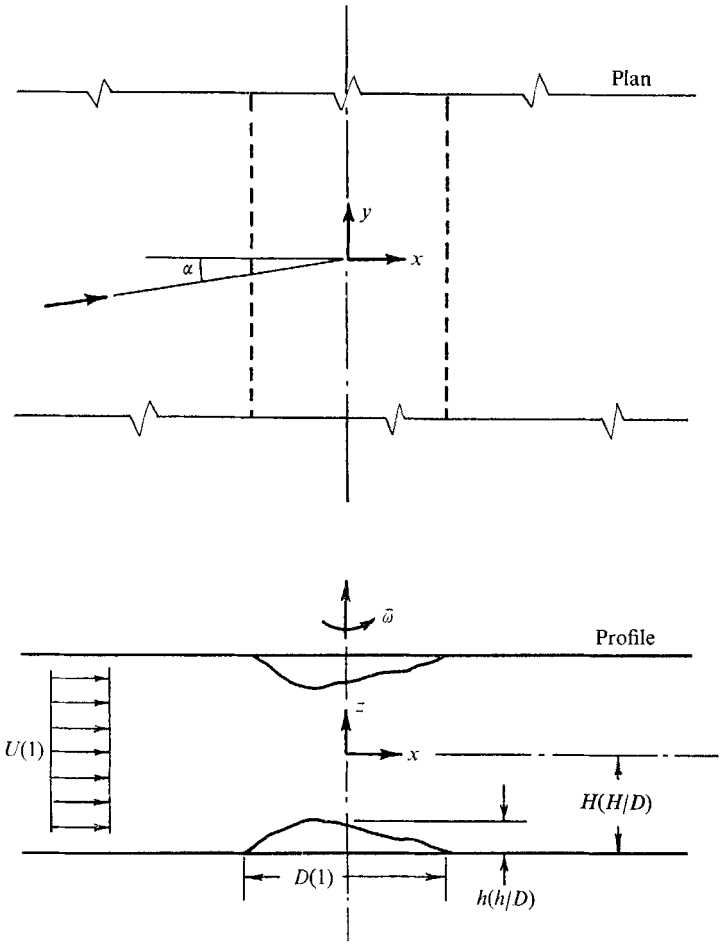

FIGURE 1. Physical system – small slope ridge study.
Dimensionless quantities are indicated by parentheses.

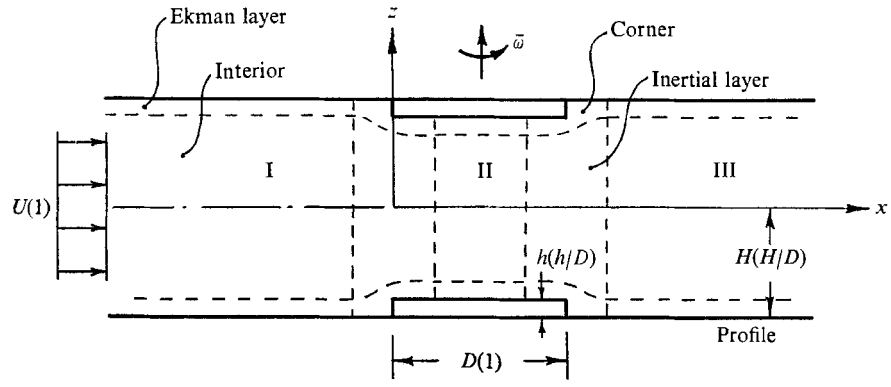

FIGURE 2. Physical system – step.
Dimensionless quantities are indicated by parentheses.

For the small slope case, the lowest order motion outside the Ekman layers on the bounding surfaces is geostrophic everywhere. This is not true for topographies with large slopes since, as shown below, the zeroth-order motion is ageostrophic in vertical shear layers of thickness $O(E^{\frac{1}{4}})$. These layers occur in the vicinity of vertical planes defined by the large slope portions of the topography; see, for example, figure 2. The flow is ageostrophic in the shear layers because the inertial terms cannot be neglected. As such we will refer to these vertical shear layers as 'inertial layers'.

The remaining portions of the flow field away from the bounding surfaces are geostrophic to lowest order. Ekman layers occur on the bounding surfaces except in corner regions where the inertial and Ekman layers intersect (figure 2). The general aim of the analysis is to determine the lowest order motion in the geostrophic regions and then to compare these results with experiment. With this limited objective, it is unnecessary to determine the detailed structure of either the inertial layers or the corner regions.

It should be noted at the outset that if one restricts to a non-inertial flow (i.e. zero Rossby number) the problem as defined can be solved by using an analysis almost identical to that given by Moore & Saffman (1969). Under this assumption the flow field again consists of three geostrophic regions (figure 2), but now the shear layers defined by the edges of the step are Stewartson layers.

Since the flow in the geostrophic regions is irrotational and since, in addition, the flow field is assumed to be independent of the co-ordinate along the axis of the step system, it is easily shown that the streamlines are straight in these regions. The indeterminateness of the flow in the geostrophic regions is then removed by matching with the Stewartson layers; e.g. see Moore & Saffman.

A horizontal streamline predicted for a non-inertial flow is sketched in figure 3; note that the streamline pattern is independent of the co-ordinate measured along the ridge. Downstream of the ridge the streamline is shifted a distance S to the right (facing downstream) of its upstream direction. It is easily shown that

$$S = 2^{\frac{1}{2}}(h/D)\, E^{-\frac{1}{2}} \cos\alpha.$$

It is important to note that for the non-zero Rossby number theory developed below, the solution obtained approaches the non-inertial solution as $k \to 0$ (i.e. $Ro \to 0$). It is found that S as predicted by the inertial theory is independent of Ro and is the same as that given by (1.2); i.e. the streamline shift does not depend on inertial effects. On the other hand the streamline patterns predicted for non-zero Ro in the vicinity of the step are quite different from those obtained for the non-inertial theory (figure 3).

With the present laboratory apparatus it is not possible to experiment in the range of validity of the non-inertial theory. Experiments can, however, be conducted for the inertial case, as defined by (1.1). Under these conditions the theory advanced is found to be in good agreement with experiment.

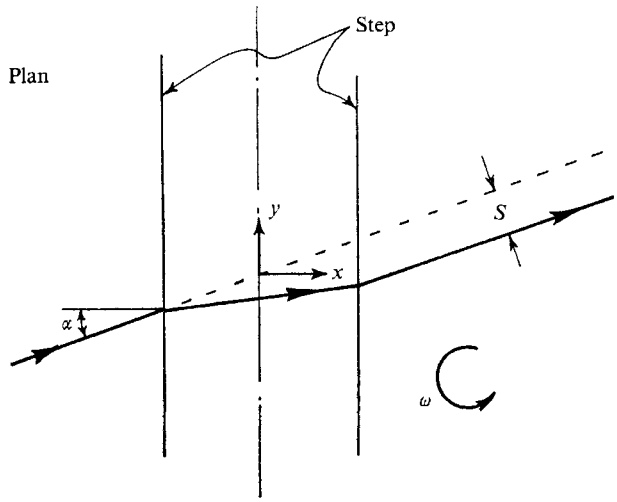

FIGURE 3. Interior streamline pattern for a non-inertial flow (i.e. $Ro = 0$).

2. Scaling and analysis

We assume that the flow is steady and that the step is infinitely long (i.e. so that the velocity field is independent of the y co-ordinate). The dimensionless momentum and continuity equations are then given by

$$\left.\begin{aligned} kE^{\frac{1}{2}}(uu_x + wu_z) &= -\Phi_x + v + E(u_{xx} + u_{zz}), \\ kE^{\frac{1}{2}}(uv_x + wv_z) &= -\Phi_y - u + E(v_{xx} + v_{zz}), \\ kE^{\frac{1}{2}}(uw_x + ww_z) &= -\Phi_z \quad + E(w_{xx} + w_{zz}), \\ u_x + w_z &= 0, \end{aligned}\right\} \tag{2.1}$$

respectively, where we have utilized the relation $Ro = kE^{\frac{1}{2}}$. Here (u, v, w) are the Eulerian velocity components with respect to the (x, y, z) co-ordinate system and

$$\Phi = (-\tfrac{1}{2}\omega^2 d^2 + (p/\rho) + \phi)/2\omega UD,$$

where d is the distance from the axis of rotation, p is the pressure, ρ the density, and ϕ the gravitational potential. The velocity components have been non-dimensionalized using the free stream speed U and the co-ordinates with the step width D. For the symmetric system under consideration (figure 2) the horizontal velocity components are even, and the vertical component odd, in the vertical co-ordinate. We thus solve for $z \leqslant$ only.

Interior regions

We assume that the dependent variables in the interior regions (i.e. outside the boundary layers and corner regions) can be expanded in power series in E and further that the leading terms are given by

$$\left.\begin{aligned} u &= U_0 E^0 + U_1 E^{\frac{1}{2}} + \ldots, \\ v &= V_0 E^0 + V_1 E^{\frac{1}{2}} + \ldots, \\ w &= W_0 E^0 + V_1 E^{\frac{1}{2}} + \ldots, \\ \Phi &= \Phi_0 E^0 + \Phi_1 E^{\frac{1}{2}} + \ldots, \end{aligned}\right\} \tag{2.2}$$

where $U_0, U_1, \ldots$ and Φ_1 are assumed to be of order unity. The order of the leading terms is dictated by the method of non-dimensionalization and that of the first-order terms by the suction velocity in the Ekman layers. If we now assume that variations in the dependent variables are the same order as the variables themselves and then substitute (2.2) into (2.1), the zeroth-order equations are

$$\left.\begin{aligned} \Phi_{0x} &= V_0, \quad \Phi_{0y} = -U_0, \\ \Phi_{0z} &= 0, \quad U_{0x} + W_{0z} = 0. \end{aligned}\right\} \tag{2.3}$$

Solutions of (2.3) require that

$$U_0 = \cos\alpha, \quad V_0 = V_0(x), \quad W_0 = 0. \tag{2.4}$$

Here U_0 is determined from the upstream boundary condition. It should be noted that this is the leading term for u in all three interior regions since it is shown below that the $O(E^0)$ component of u does not change across the inertial layers. That $W_0 = 0$, is obtained from the fact that (2.3) requires w_0 to be independent of z while, as noted above, w, and hence W_0, must be odd in z.

The first-order interior equations are now given by

$$\left.\begin{aligned} \Phi_{1x} &= V_1, \quad \Phi_{1y} = -U_1 - k\cos\alpha V_{0x}, \\ \Phi_{1z} &= 0, \quad U_{1x} + W_{1z} = 0. \end{aligned}\right\} \tag{2.5}$$

Solving (2.5) for W_1 and noting that w must be odd in z one obtains

$$W_1 = kz\cos\alpha V_{0xx}. \tag{2.6}$$

We now recall from the Ekman layer analysis in Boyer (1971) that the vertical velocity component evaluated at the edge of the Ekman layers is given by $2^{-\frac{1}{2}} V_{0x} E^{\frac{1}{2}}$. This value must be equated to the interior component, (2.6), evaluated at $z = -H/D$. One thus obtains the governing equation for V_0; i.e.

$$V_{0xx} + aV_{0x} = 0, \tag{2.7}$$

where $a = 2^{-\frac{1}{2}} k\cos\alpha\,(H/D)$. Solving for V_0 one obtains

$$V_0 = A\,e^{-ax} + C, \tag{2.8}$$

where A and C are constants of integration. Substituting (2.8) into (2.5) and solving yields

$$\left.\begin{aligned} u &= \cos\alpha E^0 + (Aak\cos\alpha\, e^{-ax} + B)\,E^{\frac{1}{2}} + \ldots, \\ v &= (Ae^{-ax} + C)\,E^0 + V_1(x)\,E^{\frac{1}{2}} + \ldots, \\ w &= Aa^2 k\cos\alpha z\, e^{-ax} E^{\frac{1}{2}} + \ldots, \end{aligned}\right\} \tag{2.9}$$

where B is another constant of integration and where, for convenience, we have also included the zeroth-order terms. Note that A, B and C must be determined in each of the geostrophic regions to complete the analysis.

Far upstream of the step (region I in figure 2), the flow field must approach a uniform free stream. Thus from (2.9) one obtains

$$A_{\mathrm{I}} = 0, \quad B_{\mathrm{I}} = 0, \quad C_{\mathrm{I}} = \sin\alpha, \tag{2.10}$$

where the subscripts refer to the appropriate interior region. The lowest order solution in region I is thus complete and indicates no upstream influence due to the step.

The need for vertical shear layers at $x = x_0 = 0, 1$ now becomes apparent. If there are no shear layers it is clear that the order unity y-velocity component V_0 and shear stress V_{0x} between regions I and II and II and III, respectively, would both have to be continuous. From (2.9) and (2.10) it follows that the only solution meeting these requirements is

$$U_0 = \cos\alpha, \quad V_0 = \sin\alpha, \quad W_0 = 0, \tag{2.11}$$

for each of the geostrophic regions.

The trouble with this solution can be seen by examining the x flux of volume. The Ekman layer on the bed contributes an x flux of $O(E^{\frac{1}{2}})$ which is the same in all three regions, but that due to the geostrophic flow $U_0 = \cos\alpha$ is discontinuous by $O(h/D)$ or in view of the scaling restrictions (1.1), $O(E^{\frac{1}{2}})$. Thus u is forced to change by $O(E^{\frac{1}{2}})$ in shear layers at $x_0 = 0, 1$. But if u changes by $O(E^{\frac{1}{2}})$ across the layers, it follows from an examination of the shear layers (see below) that V_0 is continuous, but V_{0x} is discontinuous, across the layers. Hence the solution (2.11) cannot be correct to lowest order and the more general interior solutions (2.9) must be considered. Let us now examine the structure of the free shear layers.

Inertial layers

We define a stretched vertical boundary-layer co-ordinate by

$$x - x_0 = \zeta E^b \quad (b > 0),$$

where $x_0 = 0, 1$, ζ is assumed of order unity and b is to be determined. We further assume that $\partial/\partial z \sim E^0$. Now the matching condition with the interior regions requires the leading term in u to be of $O(E^0)$; i.e. in the vertical layers

$$u = \tilde{U}_0 E^0,$$

where $\tilde{U}_0$ is of order unity and where $\sim$ is used to indicate a vertical layer quantity. But if $\tilde{U}_0 = \tilde{U}_0(\zeta)$, the continuity equation, last of (2.1), requires the leading term in w to be of $O(E^{-b})$. This is clearly impossible and one concludes that $\tilde{U}_{0\zeta} = 0$. Thus the $O(E^0)$ terms of u in both the interior and vertical shear layer regions are independent of x and hence are given by $\cos\alpha$.

We now assume the following expansions in the vertical layers

$$\left.\begin{aligned} u &= \cos\alpha\, E^0 + \tilde{U}_1 E^{\frac{1}{2}} + \ldots, \\ v &= \tilde{V}_0 E^0 + \tilde{V}_1 E^c + \ldots, \\ w &= \tilde{W}_0 E^{\frac{1}{2}-b} + \ldots, \end{aligned}\right\} \tag{2.12}$$

where $\tilde{U}_1, \ldots, \tilde{W}_0$ are assumed of order unity, the orders of the second term in u and the leading term in v are indicated by the interior solutions, and the leading term in w is then obtained from the conservation of mass equation in the vertical layers. The second term in v is included for convenience at this point and will be discussed below; here c is to be determined.

It is convenient to introduce the z and y component vorticity equations. Neglecting terms of obviously higher order, these are given by

$$\left.\begin{aligned} kE^{\frac{1}{2}} u v_{xx} &= -u_x + E\, v_{xxx}, \\ kE^{\frac{1}{2}} u w_{xx} &= -v_z + E\, w_{xxx}, \end{aligned}\right\} \tag{2.13}$$

respectively.

We now show that $\tilde{V}_0 + \tilde{V}_0(\zeta, z)$; i.e. $\tilde{V}_0$ is a constant for each shear layer. Thus the y-velocity component V_0 evaluated in the geostrophic regions is continuous at $x_0 = 0, 1$. Substituting (2.12) into (2.13) we obtain

$$k\cos\alpha\tilde{V}_{0\zeta\zeta}E^{\frac{1}{2}-2b} = -\tilde{U}_{1\zeta}E^{\frac{1}{2}-b} + \tilde{V}_{0\zeta\zeta\zeta}E^{1-3b}, \tag{2.14}$$

$$k\cos\alpha\tilde{W}_{0\zeta\zeta}E^{1-3b} = -\tilde{V}_{0z} + \tilde{W}_{0\zeta\zeta\zeta}E^{\frac{3}{2}-4b}, \tag{2.15}$$

respectively.

Consider the following: (i) If inertia $\sim$ Coriolis in (2.14), then $b = 0$. This possibility must be dismissed since it does not have a boundary-layer character. (ii) If Coriolis $\sim$ viscous in (2.14), $b = \frac{1}{4}$. But then the inertial term in (2.14) is larger than the assumed leading order terms so that this balance is also not possible. (iii) If inertia $\sim$ viscous in (2.14), then $b = \frac{1}{2}$, and the balance is an inertia–viscous one in (2.15) as well. The boundary-layer equations are

$$k\cos\alpha\tilde{V}_{0\zeta\zeta} = \tilde{V}_{0\zeta\zeta\zeta}, \quad k\cos\alpha\tilde{W}_{0\zeta\zeta} = \tilde{W}_{0\zeta\zeta\zeta},$$

respectively. Solutions of these equations cannot be matched with the geostrophic solutions and hence this balance is also not a possible one. (iv) If inertia $\sim$ Coriolis in (2.15), $b = \frac{1}{3}$. The boundary-layer equations are thus

$$\tilde{V}_{0\zeta\zeta} = 0, \quad k\cos\alpha\tilde{W}_{0\zeta\zeta} = -\tilde{V}_{0z},$$

respectively. The solution for $\tilde{V}_0$ satisfying the geostrophic matching conditions is $\tilde{V}_0 =$ constant. It then follows that $\tilde{W}_0 = 0$. This balance is also impossible. (v) If Coriolis $\sim$ viscous in (2.15), then $b = \frac{3}{8}$. But now the inertial term in (2.15) is larger than the assumed leading order terms; i.e. a contradiction. (vi) Finally, if inertia $\sim$ viscous in (2.15) we are again led to (iii) which was shown to be impossible.

We conclude that the leading term for v (i.e. $\tilde{V}_0$) in the shear layer equations is a constant in each layer. Thus the y-velocity component V_0 in the geostrophic regions is continuous across the shear-layers; i.e. from (2.9) continuity of V_0 at $x_0 = 0, 1$ yields

$$A_{\mathrm{II}} + C_{\mathrm{II}} = \sin\alpha, \tag{2.16}$$

$$A_{\mathrm{II}}e^{-a} + C_{\mathrm{II}} = A_{\mathrm{III}}e^{-a} + C_{\mathrm{III}}, \tag{2.17}$$

respectively.

Return now to the shear layer expansions (2.12) where $\tilde{V}_0$ is now considered to be constant and hypothesize that the role of the shear layers is to remove the discontinuity in the shear stress between the geostrophic regions. The shear stress requirements are

$$\left.\begin{aligned}\tilde{V}_{1\zeta}(\zeta \to -\infty)E^{c-b} &= V_{0x}^{-}(x_0),\\ \tilde{V}_{1\zeta}(\zeta \to +\infty)E^{c-b} &= V_{0x}^{+}(x_0),\end{aligned}\right\} \tag{2.18}$$

where the $-$ and $+$ signs represent geostrophic regions to the left and right, respectively, of the shear layer under consideration. Clearly then, from (2.18), $b = c$.

Again substituting (2.12) into (2.13), we now obtain

$$k\cos\alpha\tilde{V}_{1\zeta\zeta}E^{\frac{1}{2}-b} = -\tilde{U}_{1\zeta}E^{\frac{1}{2}-b} + \tilde{V}_{1\zeta\zeta\zeta}E^{1-2b}, \tag{2.19}$$

$$k\cos\alpha\tilde{W}_{0\zeta\zeta}E^{1-3b} = -\tilde{V}_{1z}E^{b} + \tilde{W}_{0\zeta\zeta\zeta}E^{\frac{3}{2}-4b}. \tag{2.20}$$

We now consider the possible balancing of terms in (2.19) and (2.20) subject to the constraints of the geostrophic motion: (i) If in (2.19) inertia, Coriolis $\sim$ viscous then $b = \frac{1}{2}$. From (2.20) this leads to the boundary-layer equation

$$\tilde{W}_{0\zeta\zeta\zeta} - k\cos\alpha\tilde{W}_{0\zeta\zeta} = 0.$$

The only solution of this equation satisfying the interior matching conditions on $\tilde{W}_0$ is $\tilde{W}_0 = 0$. This scaling is thus not a possible one. (ii) If in (2.20) Coriolis $\sim$ viscous, we find $b = \frac{3}{10}$. There is a contradiction, however, since the neglected inertial term is of lower order than the assumed leading order terms. (iii) The only remaining possibility is that inertia $\sim$ Coriolis in (2.20). This leads to $b = \frac{1}{4}$ and thus the balance is also an inertia–Coriolis one in (2.19). The resulting inertial boundary-layer equations are given by

$$\left.\begin{aligned} k\cos\alpha\,\tilde{V}_{1\zeta\zeta} &= -\tilde{U}_{1\zeta}, \\ k\cos\alpha\tilde{W}_{0\zeta\zeta} &= -\tilde{V}_{1z}, \\ \tilde{U}_{1\zeta} + \tilde{W}_{0z} &= 0, \end{aligned}\right\} \tag{2.21}$$

where the continuity relation has also been included.

The Ekman compatibility condition combined with the above scaling requires

$$\tilde{W}_0(z = -H/D) = 0. \tag{2.22}$$

The situation here is similar to that discussed by Moore & Saffman in that it seems that (2.22) does not allow a transport from the Ekman layers into the inertial layers. What it really implies, however, is that fluid is transported from the Ekman layers into the inertial layers in a region of width $O(E^{\frac{1}{4}})$, a source with respect to the inertial layers. The singular behaviour is associated with the edge of the step.

While the boundary-layer equations (2.21) can be solved subject to the appropriate matching conditions imposed by the geostrophic motion and the boundaries $z = 0$ and $z = -H/D$, it is not necessary to carry out this analysis in order to determine the solution in the geostrophic regions. We now use a procedure similar to that introduced by Stewartson (1966) and then used by Moore & Saffman. We first use the continuity relation to eliminate $\tilde{U}_{1\zeta}$ in the first of (2.21) and then we integrate the resulting equation across the inertial layer for a fixed z; i.e.

$$\int_{-\infty}^{\infty} \{k\cos\alpha V_{1\zeta\zeta} = \tilde{W}_{0z}\}\,d\zeta,$$

or

$$k\cos\alpha\{\tilde{V}_{1\zeta}(\zeta\to+\infty) - \tilde{V}_{1\zeta}(\zeta\to-\infty)\} = \frac{\partial}{\partial z}\int_{-\infty}^{\infty}\tilde{W}_0\,d\zeta.$$

Using (2.18) and integrating from $z = 0$ to $z = -H/D$ we then obtain

$$k(H/D)\cos\alpha\{V_{0x}^{-}(x_0) - V_{0x}^{+}(x_0)\} = \int_{-\infty}^{\infty}\tilde{W}_0(z = -H/D)\,d\zeta. \tag{2.23}$$

Consider now the mass transport through the corner region near $x_0 = 0$ as sketched in figure 4. The width of the region considered is that of the inertial layers, $O(E^{\frac{1}{4}})$, and the height is taken as $O(E^{\beta})$ where $0 < \beta < \frac{1}{2}$. The lower limit on β is required so that relation (2.23) can be utilized and the upper limit ensures

that the upper boundary of the region is outside of the Ekman layers. From the geostrophic solutions and attendant Ekman layer equations we find that the net transport per unit length across the vertical surfaces of the corner region is given by

$$\text{In} - \text{Out} = h_0 \cos\alpha \, E^{\frac{1}{2}}. \tag{2.24}$$

Note that, for the corner region near $x_0 = 1$, the sign of the right-hand side of (2.24) is negative. This net transport must equal the transport across the horizontal surface as given by (2.23) and thus

$$V_{0x}^{-}(x_0) - V_{0x}^{+}(x_0) = \pm (h_0/k)(D/H), \tag{2.25}$$

where the upper sign is for $x_0 = 0$ and the lower for $x_0 = 1$.

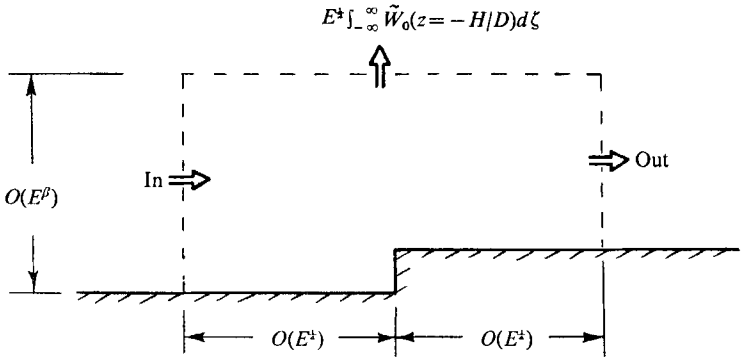

FIGURE 4. Corner region transport.

Applying (2.25) to the interior equations, (2.9) yields the desired solution; i.e. applying (2.25) at $x_0 = 0$ and $x_0 = 1$ we find

$$A_{\text{II}} = 2^{\frac{1}{2}} h_0 \cos\alpha, \tag{2.26}$$

$$e^{-a}(A_{\text{III}} - A_{\text{II}}) = -2^{\frac{1}{2}} h_0 \cos\alpha, \tag{2.27}$$

respectively. Solving (2.16), (2.17), (2.26), and (2.27) one obtains

$$\left.\begin{aligned} A_{\text{II}} &= 2^{\frac{1}{2}} h_0 \cos\alpha, & C_{\text{II}} &= \sin\alpha - 2^{\frac{1}{2}} h_0 \cos\alpha, \\ A_{\text{III}} &= 2^{\frac{1}{2}} h_0 \cos\alpha\,(1-e^{a}), & C_{\text{III}} &= \sin\alpha. \end{aligned}\right\} \tag{2.28}$$

Thus the leading order velocity components in the interior have been determined. By equating the x mass transport to $O(E^{\frac{1}{2}})$ across planes parallel to the y, z plane in each of the three geostrophic regions one finds that $B_{\text{II}} = B_{\text{III}} = 0$. Thus the second-order interior term in u has also been determined.

The lowest order horizontal streamline pattern is now obtained by integrating the relation $U_0 dy = V_0 dx$. The resulting equation for the streamline passing through the origin is given by

$$y = \left\{\begin{aligned} &x\tan\alpha, && (x \leqslant 0) \\ &x\tan\alpha + (2^{\frac{1}{2}} h_0/a)\{1 - ax - e^{-ax}\}, && (0 \leqslant x \leqslant 1) \\ &x\tan\alpha - (2^{\frac{1}{2}} h_0/a)\{a + (1-e^{a})\, e^{-ax}\}, && (x \geqslant 1). \end{aligned}\right\} \tag{2.29}$$

Examples of these streamlines for $\alpha = 0$ are plotted in figure 5. The flow characteristics, as might be expected, are qualitatively similar to those discussed in Boyer

1971). There is no upstream influence and downstream of the ridge the streamlines are shifted a distance S to the right, facing downstream, where

$$S = 2^{\frac{1}{2}}(h/D)\,E^{-\frac{1}{2}}\cos\alpha. \tag{2.30}$$

Note that as $k \to 0$ or $a \to \infty$ (i.e. $Ro \to 0$) in (2.29), the streamline pattern approaches that given by the non-inertial analysis discussed earlier (figure 3). It should again be emphasized that while the downstream shift S does not depend on inertial effects, the streamline characteristics in the vicinity of the step are strongly dependent on these effects.

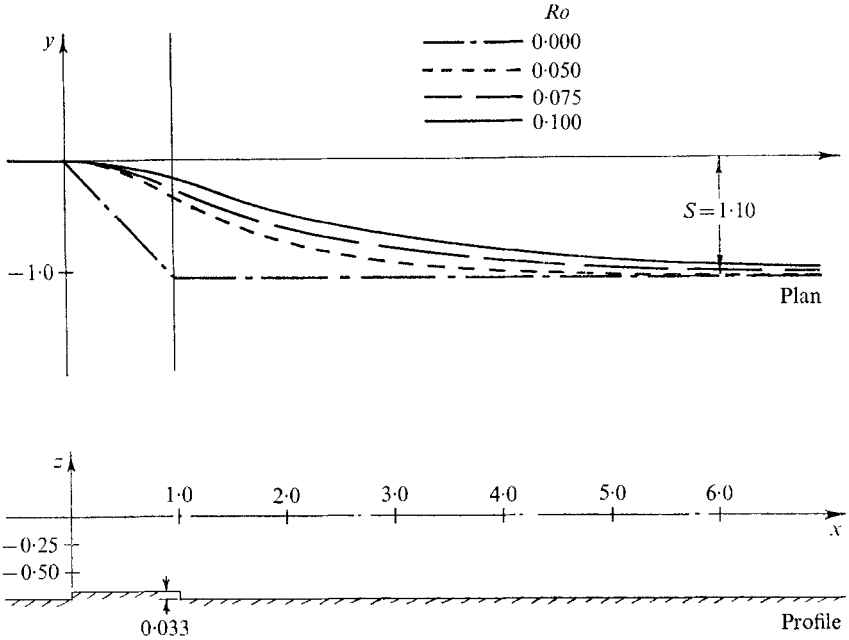

FIGURE 5. Interior streamlines–theoretical. The flow is from left to right and the rotation is counterclockwise. $E = 1{\cdot}8(10)^{-5}$, $H/D = 0{\cdot}750$, $h/D = 0{\cdot}033$, $\alpha = 0$.

In the experiments discussed below a step topography of finite length is considered; i.e. the step is confined laterally by vertical walls. Thus from an experimental standpoint it would be desirable to obtain a theoretical solution for the flow over a step system located on the upper and lower walls of a channel of finite width. This is not an easy task, however, at least for the inertial problem. Such a solution has thus not been attempted. The difficulties are two-fold. In the first place the governing equation for the stream function ψ, in the geostrophic regions would contain the non-linear inertial term $J(\psi, \nabla^2\psi)$, where J is the Jacobian. Numerical solutions would thus have to be sought. The second difficulty is a numerical one, since it is by no means obvious just how to incorporate a boundary condition such as that given by (2.25) into a numerical scheme.

3. Experimental results

The above theory can be compared with experiment by using a rotating water tunnel. The basic capability of the tunnel is that it can provide a uniform flow relative to a rotating observer. Step topographies can thus be placed in the flow

as indicated in figure 2 and the resulting motion can be examined using dye tracer techniques. Since the details of the rotating apparatus have been described elsewhere (Boyer 1971), they will not be repeated here. The experimental parameters and/or ranges investigated in the present study are given in table 1.

Since the water tunnel is only 35 cm wide, it becomes important to choose the experimental parameters carefully so that the flow in the central portions of the tunnel approximates that for an infinite step. Placing an upper limit of 5 cm on the predicted downstream shift S was found to be a satisfactory criterion in this regard.

$D = 2{\cdot}54$ cm	$0{\cdot}1 < U < 0{\cdot}5$ cm/sec
$H = 1{\cdot}905 \pm 0{\cdot}008$ cm	$0{\cdot}5 < \omega < 1{\cdot}5$ rad/sec
$h = 0{\cdot}084 \pm 0{\cdot}005$ cm	$9{\cdot}0(10)^{-3} < \nu < 9{\cdot}4(10)^{-3}$ cm^2/sec
$H/D = 0{\cdot}750$	$5{\cdot}0(10)^{-4} < E < 2{\cdot}0(10)^{-3}$
$h/D = 0{\cdot}033$	$0{\cdot}02 < Ro < 0{\cdot}20$
$\alpha = 0^0$	

TABLE 1

Figure 6 (plate 1) is a photograph of an experiment in which a tracer has been released from a series of lateral positions upstream of the step and in the midplane ($z = 0$) of the tunnel. Since the flow is steady, these streaklines depict the streamlines of the flow. It is clear from the photograph that there is good qualitative agreement with the theory. For example, there is little discernable upstream influence, the flow in the vicinity of the step is similar to that predicted and there is a net displacement to the right far downstream. The quantitative agreement is also quite good as indicated by the theoretical streamline sketched on the photograph. Note that far downstream of the step the streamlines again curve toward the left. This return leftward curvature is attributed to side wall effects in the tunnel.

Figure 7 is a plot of the maximum downstream shift S as a function of the lateral co-ordinate y for the experimental run given in figure 6. This plot clearly shows that the side walls affect the streamline pattern in the vicinity of the tunnel walls. The effect is relatively small in the central portion of the flow field, however, and thus the assumption of a step of infinite length is a reasonable one in this region.

In order to quantitatively compare theory and experiment, for a series of experiments, runs were conducted in which E, h/D and H/D were fixed and Ro was varied. The maximum shift S was then measured and compared with the theoretical value given by (2.30). Figure 8 demonstrates the results of two such series of experiments. One first notes that there clearly is a Rossby number dependence for S; this is in apparent opposition to the theory. Discrepancies of the order noted should be expected, however, since terms of $O(Ro)$ have been neglected in the theoretical development. Note that the agreement improves as the Rossby number is reduced and hence the experiments are consistent with the theory in this regard.

It should be noted that various experimental errors may also contribute to the discrepancies between theory and experiment. These include, for example, side wall effects, horizontal shear in the free stream flow, non-neutrally buoyant tracer effects, errors in velocity measurements and errors in geometry. The latter effect became especially apparent in the present study in that gap widths (i.e. H and $H-h$) had to be accurate to within 0·1 mm if satisfactory flows were to be obtained.

As a final experiment the pH technique discussed by Baker (1966) was used to examine the structure of the vertical velocity field in a qualitative way. The

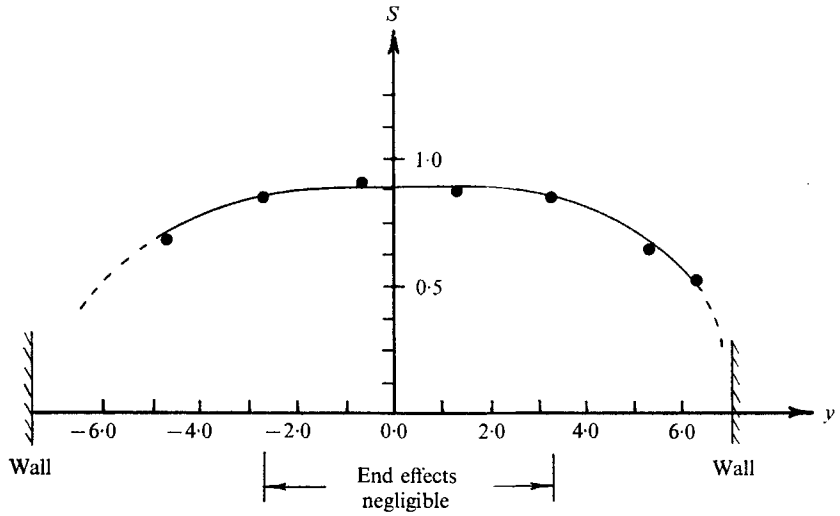

FIGURE 7. Lateral variation of the downstream shift for the experimental run given in figure 6.

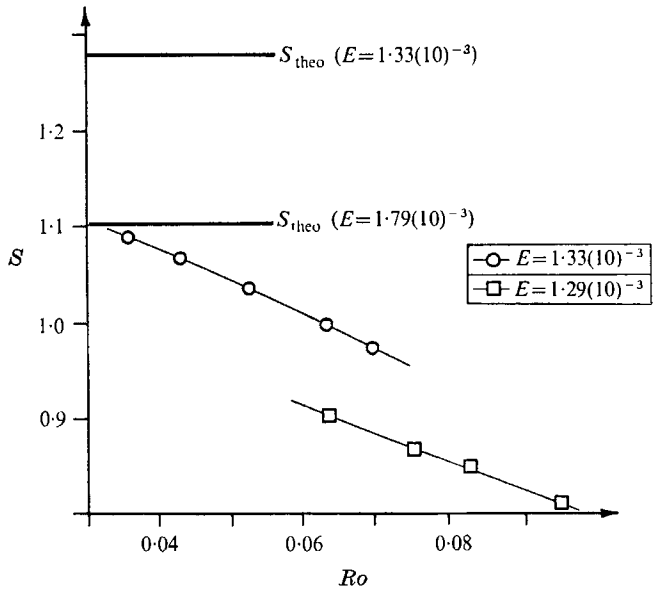

FIGURE 8. Downstream shift *vs.* Rossby number. $H/D = 0{\cdot}750$, $h/D = 0{\cdot}033$, $\alpha = 0$.

experiment performed is indicated schematically in figure 9(*c*) (plate 2). Here a tracer was released at a distance of 1·27 cm upstream of the ridge and at a height of 0·95 cm above the floor of the tunnel. The lateral location of the tracer source was 8 cm from the vertical wall on the left facing downstream. Two horizontal reference wires were positioned as indicated.

Figure 9(*b*) (plate 2) is a photograph of an experiment. The reference wires are clearly indicated by the dark horizontal lines and the tracer streakline by the somewhat wavy light line. The top of the lower step is indicated by the light horizontal line near the bottom of the photo. An exaggerated interpretive streakline is given in figure 9(*c*).

Figure 9(*a*) is a plot of the theoretical vertical velocity field in the geostrophic regions for the parameters indicated; the calculations are made at the fixed height at which the tracer is released. The vertical velocity field in the shear layers is indicated schematically by the dashed lines. Since $E \sim O(10^{-4})$ in the experiment and since the free stream velocity is of order unity, the streakline slope should be $O(10^{-1})$ in the inertial layers and $O(10^{-2})$ in the geostrophic regions.

We can make the following observations from the experiment: (i) The streakline is relatively flat upstream of the step. This agrees with theory since the Ekman suction velocity here should be zero. (ii) In the vicinity of the forward face of the step the streakline has a relatively large positive slope. This is in agreement with the $O(E^{\frac{1}{4}})$ positive vertical velocity near $x_0 = 0$ as discussed earlier. (iii) Over the step the Ekman suction velocity is negative as indicated in figure 9(*a*) and thus the streakline should slope downward slightly as shown. (iv) Near the downstream face of the step the streakline has a relatively large negative slope. This also should be expected since there is an $O(E^{\frac{1}{4}})$ suction into the corner near $x_0 = 1$ as previously described. (v) While the theory predicts a positive vertical velocity from Ekman layer pumping downstream of the step (figure 9(*a*)), a positive streakline slope is not apparent in the photograph.

In summary an inertial theory for flow over a step of infinitesimal amplitude has been advanced; the theoretical restrictions are delineated in relations (1.1). Experiments have also been presented which are in good agreement with the theory.

The author would like to thank Mr Earle Gould for conducting the experiments. This work was supported jointly by the National Science Foundation under Grant GA-943 and by Project THEMIS.

REFERENCES

BAKER, D. J. 1966 A technique for the precise measurement of small fluid velocities. *J. Fluid Mech.* **26**, 573.

BOYER, D. L. 1971 Rotating flow over long shallow ridges. *Geophysical Fluid Dynamics*, **2**, 185.

MOORE, D. W. & SAFFMAN, P. G. 1969 The flow induced by the transverse motion of a thin disk in its own plane through a contained rapidly rotating viscous liquid. *J. Fluid Mech.* **39**, 831.

STEWARTSON, K. 1966 On almost rigid rotations. Part 2. *J. Fluid Mech.* **26**, 131.

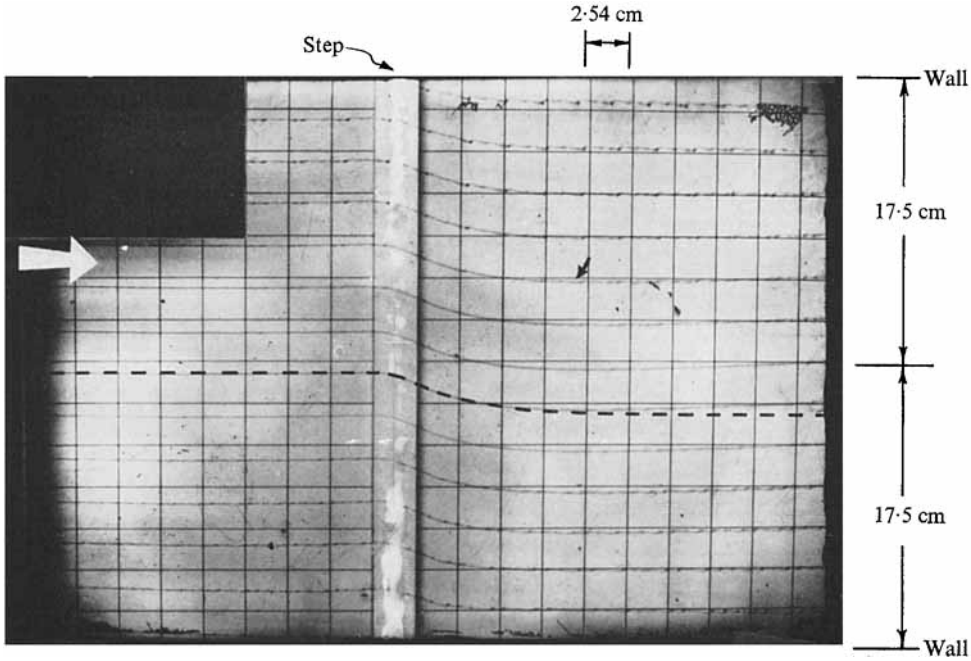

FIGURE 6. Midplane streamlines–experimental; a theoretical streamline is indicated by the dashed line. The flow is from left to right and the rotation is counterclockwise. $E = 1{\cdot}79(10)^{-4}$, $Ro = 7{\cdot}5(10)^{-2}$, $H/D = 0{\cdot}75$, $h/D = 0{\cdot}033$, $\alpha = 0$.

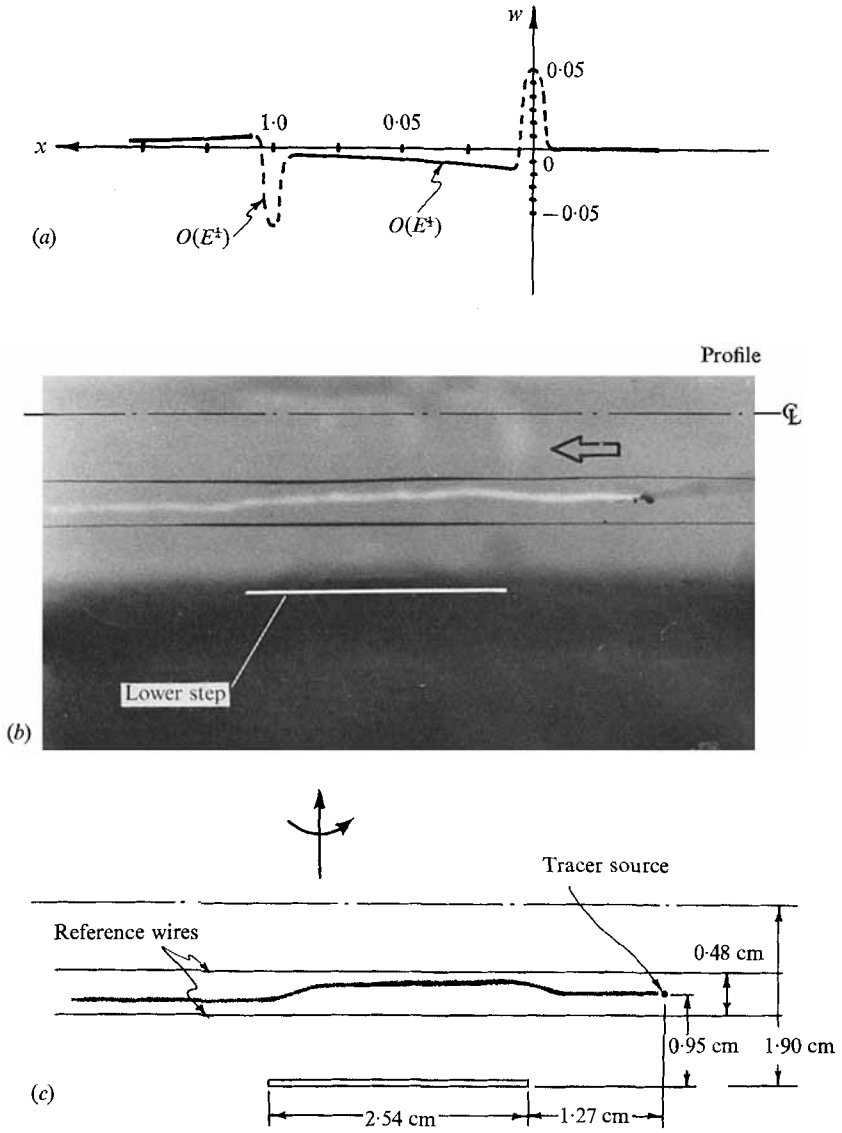

FIGURE 9. Experiment demonstrating the vertical velocity field in the vicinity of the step; $E = 3{\cdot}2(10)^{-4}$, $Ro = 1{\cdot}4(10)^{-2}$, $H/D = 0{\cdot}75$, $h/D = 0{\cdot}033$. (*a*) Vertical velocity profile evaluated at $z = -\frac{1}{2}H$. (*b*) Experiment. (*c*) Interpretive sketch.